LHCb-CONF-2023-003
October 23, 2023

Study of *CP*-violation in $B^0 \to DK^*(892)^0$ decays with $D \to K\pi(\pi\pi)$, $\pi\pi(\pi\pi)$, and KK final states

LHCb collaboration[†]

Abstract

The *CP*-violating observables associated with the interference of $B^0 \to D^0 K^*(892)^0$ and $B^0 \to \overline{D}{}^0 K^*(892)^0$ decay amplitudes are measured in the $D^0 \to K^\mp\pi^\pm(\pi^+\pi^-)$, $D^0 \to \pi^+\pi^-(\pi^+\pi^-)$, and $D^0 \to K^+K^-$ final states with proton-proton data collected by the LHCb experiment corresponding to an integrated luminosity of $9\,\text{fb}^{-1}$. These observables are used to set constraints on the parameter space of the CKM angle γ and the hadronic parameters $r_{B^0}^{DK^*}$ and $\delta_{B^0}^{DK^*}$ with inputs from other measurements. These new measurements allow for four solutions in the parameter space, but only one is consistent with the world-average determination of γ.

© 2023 CERN for the benefit of the LHCb collaboration. CC BY 4.0 licence.

[†]Conference report prepared for the 12th international workshop on the CKM Unitarity Triangle, Santiago, Spain, 18–22 September 2023. Contact authors: Alex Gilman, alex.gilman@physics.ox.ac.uk and Sneha Malde, sneha.malde@physics.ox.ac.uk.

LHCb-CONF-2023-003
24/10/2023

1 Introduction

The only observed phenomena of *CP* violation are attributed to complex phases in the Cabibbo-Kobayashi-Maskawa (CKM) matrix elements [1,2], which describe the interactions mediated by $W^{\pm}$ bosons between quarks of different flavour and form a three-by-three unitary matrix. A corollary to CKM unitarity provides a set of Pythagorean relations between the matrix elements. One such relation, particularly relevant to decays of B^0 mesons, is commonly parameterised in terms of three angles α, β, and γ which sum to 180°. The angle γ can be measured from the interference of $b \to c\overline{u}s$ and $b \to \overline{c}us$ amplitudes with negligible theoretical uncertainties [3]. Precise measurements of γ provide strong tests of the Standard Model's requirement of CKM unitarity and thus its description of *CP* violation.

The value of γ can be determined indirectly by assuming CKM unitarity and performing a global fit to all measurements relating to the CKM matrix. With such techniques, the UTFit collaboration determined $\gamma = (64.9 \pm 1.4)^{\circ}$ [4] and the CKMFitter collaboration determined $\gamma = \left(65.5^{+1.3}_{-1.2}\right)^{\circ}$ [5]. The determination of γ through direct measurements of $b \to c\overline{u}s$ and $b \to \overline{c}us$ interference is currently driven by the LHCb experiment. The world average of direct measurements from HFLAV is $\gamma = \left(66.2^{+3.4}_{-3.6}\right)^{\circ}$ [6], and is dominated by $B^+ \to DK^+$ decays that have been analysed with all of the available LHCb data [7]. Here and throughout the article, D is used to represent a superposition of D^0 and $\overline{D}^0$ decays to the previously listed final states, with a similar convention for D^*. While the results of the direct and indirect determinations of γ are in agreement, the comparison is completely limited by the precision of direct measurements. As such, additional direct measurements of γ are required to provide more stringent tests of CKM unitarity. Despite the smaller branching fraction of $B^0 \to DK^*(892)^0$ decays, a competitive precision on γ can be achieved due to the larger interference effects in these decays compared to B^+ decays [8]. The *CP* violation in these decays only depends on the flavour at decay, and thus can be studied independent of decay time.

This article presents the measurement of *CP*-violating observables in the decays of $B^0 \to DK^*(892)^0$ in the $D \to K^{\mp}\pi^{\pm}$, K^+K^-, $\pi^+\pi^-$, $K^{\mp}\pi^{\pm}\pi^+\pi^-$, and $\pi^+\pi^-\pi^+\pi^-$ decay modes with proton-proton collision data at centre-of-mass energies between 7 and 13 TeV collected by the LHCb detector in 2011-2012 (Run1) and 2015-2018 (Run2), corresponding to an integrated luminosity of 9 fb^{-1}. The $K^*(892)^0$ meson is referred to throughout as K^{*0} and is implied to decay to a $K^+\pi^-$ final state. The interpretation of these *CP*-violating observables in terms of γ and hadronic parameters for $B^0 \to DK^*(892)^0$ decays is also presented. This work examines the ADS final states, which realise interference in the admixture of Cabibbo-favoured and doubly Cabibbo suppressed $D^0 \to K^-\pi^+(\pi^+\pi^-)$ and $\overline{D^0} \to K^-\pi^+(\pi^+\pi^-)$ decays [9]. The notation $K\pi(\pi\pi)$ is used to refer to the final state where the kaon child of the D candidate has the same charge as the kaon child of the K^* candidate, and $\pi K(\pi\pi)$ to refer to the final state where the two kaons have opposite charge. The *CP*-eigenstate final states $D \to \pi^+\pi^-$ and $D \to K^+K^-$ are also studied and referred to as GLW decay modes [10, 11]. An extension to the GLW method [12] allows the inclusion of the $D \to \pi^+\pi^-\pi^+\pi^-$ decay mode which is predominantly *CP*-even.

These two classes of final states provide complementary sensitivity to the funda-

mental parameters of interest: the weak phase, γ, the ratio of amplitudes between the $B^0 \to \overline{D}^0 K^{*0}$ and $B^0 \to D^0 K^{*0}$ decays, $r_{B^0}^{DK^*}$, and the strong phase difference between the two amplitudes, $\delta_{B^0}^{DK^*}$. The interference can introduce asymmetries in the rates between $\overline{B}^0 \to D\overline{K}^{*0}$ and $B^0 \to DK^{*0}$ decays, and modulate the charge-integrated decay rates of $B^0 \to DK^{*0}$ for each D meson decay. The effects of interference in the $B^0 \to D[K\pi(\pi\pi)]K^{*0}$ final state are expected to be small compared to the predicted experimental sensitivity, and so this final state is used as a normalisation channel to probe interference effects in the other final states. This strategy also provides the benefit of the cancellation of a large number of systematic uncertainties related to the reconstruction and selection of signal candidates. For the $B^0 \to D[\pi K(\pi\pi)]K^{*0}$ final state, the parameters

$$\mathcal{R}^{+}_{\pi K(\pi\pi)} \equiv \frac{\Gamma\left(B^0 \to D\left[\pi K(\pi\pi)\right] K^{*0}\right)}{\Gamma\left(B^0 \to D\left[K\pi(\pi\pi)\right] K^{*0}\right)} \quad \text{and} \quad \mathcal{R}^{-}_{\pi K(\pi\pi)} \equiv \frac{\Gamma\left(\overline{B}^0 \to D\left[\pi K(\pi\pi)\right] \overline{K}^{*0}\right)}{\Gamma\left(\overline{B}^0 \to D\left[K\pi(\pi\pi)\right] \overline{K}^{*0}\right)} \tag{1}$$

are measured. The asymmetry of the $B^0 \to D[K\pi(\pi\pi)]K^{*0}$ final state

$$\mathcal{A}_{K\pi} \equiv \frac{\Gamma\left(\overline{B}^0 \to D[K\pi(\pi\pi)]\overline{K}^{*0}\right) - \Gamma\left(B^0 \to D[K\pi(\pi\pi)]K^{*0}\right)}{\Gamma\left(\overline{B}^0 \to D[K\pi(\pi\pi)]\overline{K}^{*0}\right) + \Gamma\left(B^0 \to D[K\pi(\pi\pi)]K^{*0}\right)} \tag{2}$$

is also measured.

For the GLW final states, the flavour-integrated decay rates relative to the $B^0 \to D[K\pi(\pi\pi)]K^{*0}$ are measured, but the asymmetries are self normalising, so the observables of interest are

$$\mathcal{R}_{CP}^{hh(\pi\pi)} \equiv \frac{\Gamma(\overline{B}^0 \to D[hh(\pi\pi)]\overline{K}^{*0}) + \Gamma(B^0 \to D[hh(\pi\pi)]K^{*0})}{\Gamma(\overline{B}^0 \to D[K\pi(\pi\pi)]\overline{K}^{*0}) + \Gamma(B^0 \to D[K\pi(\pi\pi)]K^{*0})} \times \frac{\mathcal{B}(D^0 \to K\pi(\pi\pi))}{\mathcal{B}(D^0 \to hh(\pi\pi))} \tag{3}$$

and

$$\mathcal{A}_{CP}^{hh(\pi\pi)} \equiv \frac{\Gamma\left(\overline{B}^0 \to D[hh(\pi\pi)]\overline{K}^{*0}\right) - \Gamma\left(B^0 \to D[hh(\pi\pi)]K^{*0}\right)}{\Gamma\left(\overline{B}^0 \to D[hh(\pi\pi)]\overline{K}^{*0}\right) + \Gamma\left(B^0 \to D[hh(\pi\pi)]K^{*0}\right)}, \tag{4}$$

where $hh(\pi\pi)$ refers to KK, $\pi\pi$, or $\pi\pi\pi\pi$.

The decay $B_s^0 \to D\overline{K}^{*0}$ can be parameterised in an identical fashion, and given the similar decay topology, the *CP*-violating observables of this process are also measured in this analysis. However, the effect of the interference in this process is expected to be negligible in all of the observed decay modes, as the parameter directly proportional to the interference effects, $r_{B_s^0}^{DK^*}$, is estimated to be roughly an order of magnitude smaller than the corresponding B^0 parameter based on the known CKM elements [6]. Similar notation is used to refer to the B_s^0 observables throughout the article, with an additional s in the subscript.

All of these observables have been measured previously by the LHCb collaboration using the data collected in Run1 and 2015-2016, except the ones associated with the $D \to \pi\pi\pi\pi$ decay channel, for which only the 2015-2016 data was analysed [13]. The measurements presented in this article supersede the results of the previous analysis.

The rest of the article is organised as follows. The LHCb detector and simulation is described in Sect. 2. The selection requirements placed on signal candidates are discussed

in Sect. 3. The determination of *CP*-violating observables from the signal candidates passing selection requirements is discussed in Sect. 4. The interpretation of the determined *CP*-violating observables in terms of the fundamental physics parameters and concluding remarks are presented in Sect. 5.

2 LHCb detector & simulation

The LHCb detector [14,15] is a single-arm forward spectrometer covering the pseudorapidity range $2 < \eta < 5$, designed for the study of particles containing b or c quarks. The detector includes a high-precision tracking system consisting of a silicon-strip vertex detector surrounding the pp interaction region [16], a large-area silicon-strip detector located upstream of a dipole magnet with a bending power of about 4 Tm, and three stations of silicon-strip detectors and straw drift tubes [17] placed downstream of the magnet. The tracking system provides a measurement of the momentum, p, of charged particles with a relative uncertainty that varies from 0.5% at low momentum to 1.0% at 200 GeV/c. The minimum distance of a track to a primary pp collision vertex (PV), the impact parameter (IP), is measured with a resolution of $(15 + 29/p_{\rm T})$ μm, where $p_{\rm T}$ is the component of the momentum transverse to the beam, in GeV/c. Different types of charged hadrons are distinguished using information from two ring-imaging Cherenkov (RICH) detectors [18, 19]. Photons, electrons and hadrons are identified by a calorimeter system consisting of scintillating-pad and preshower detectors, an electromagnetic and a hadronic calorimeter. Muons are identified by a system composed of alternating layers of iron and multiwire proportional chambers [20].

The events considered in the analysis are triggered at the hardware level either when one of the final-state tracks of the signal decay deposits enough energy in the calorimeter system, or when one of the other particles in the event, not reconstructed as part of the signal candidate, fulfils any trigger requirement. At the software level, it is required that at least one particle should have high $p_{\rm T}$ and high $\chi^2_{\rm IP}$, where $\chi^2_{\rm IP}$ is defined as the difference in the PV fit χ^2 with and without the inclusion of that particle. A multivariate algorithm [21] is used to identify displaced vertices consistent with being a two-, three-, or four-track b-hadron decay. The PVs are fitted with and without the B candidate tracks, and the PV that gives the smallest $\chi^2_{\rm IP}$ is associated with the B candidate.

Simulation is required to model the reconstructed mass distributions of the signal and background contributions and determine their selection efficiencies. In the simulation, proton-proton collisions are generated using Pythia [22] with a specific LHCb configuration [23]. Decays of unstable particles are described by EvtGen [24], in which final-state radiation is generated using Photos [25]. The simulation of interactions of the generated particles with the detector and its response is implemented using the Geant4 toolkit [26, 27] as described in Ref. [28]. Some subdominant sources of background are generated with RapidSim, a fast simulation [29] that mimics the geometric acceptance and tracking resolution of the LHCb detector as well as the dynamics of the decay via EvtGen.

3 Selection, efficiencies, and asymmetries

Signal B meson candidates are built from a $K^{*0} \to K^+\pi^-$ candidate and a D meson candidate. Selection requirements consistent with those from [30] are placed on the $K^{*0} \to K^+\pi^-$ candidate to isolate the K^{*0} resonance: the reconstructed mass of the K^{*0} candidate must be within $50\,\mathrm{MeV}/c^2$ of the known K^{*0} meson mass [31] and a requirement is made on the angle θ^* between the K^{*0} kaon child momentum and the B^0 candidate in the K^{*0} rest frame of $\cos(\theta^*) > 0.4$. The reconstructed mass of the D candidate is required to be within $25\,\mathrm{MeV}/c^2$ of the known D^0 meson mass [31].

With the above selections in place, boosted decision trees classifiers with gradient boost (BDT) [32] are trained to discriminate between signal candidates and combinatorial background. Two BDT classifiers are trained for each final state, one for each run period. The same BDT classifier is shared for each run period between the $B^0 \to [K\pi(\pi\pi)]K^{*0}$ and $B^0 \to [\pi K(\pi\pi)]K^{*0}$ final states. This gives ten separate BDT classifiers in total, each trained using simulated signal samples and background samples from data with a B^0 candidate reconstructed mass within $5800 - 5960$ MeV/c^2. The classifiers are trained using the angle between the direction of the reconstructed B momentum and the direction defined by the primary and secondary vertices, the χ^2_{IP} of the B^0 and D candidates, the reduced χ^2 of the B^0 vertex fit, the χ^2_{IP} and the transverse momenta of the K^{*0} candidate children, the χ^2_{IP} and the transverse momenta of the D candidate children (only for two-body D final states), and the transverse momentum imbalance of the B^0 candidate, defined as

$$I_{p_{\mathrm{T}}} \equiv \frac{p_{\mathrm{T}}(B^0) - \sum_X p_{\mathrm{T}}(X)}{p_{\mathrm{T}}(B^0) + \sum_X p_{\mathrm{T}}(X)}, \tag{5}$$

where the summation is over all charged tracks X inconsistent with originating from the primary vertex within a cone around the B^0 candidate, excluding those used in the B^0 reconstruction. Variables related to the D children are omitted for the four-body D final states to avoid any dependence on the modelling of the D decay dynamics. Requirements on the output of each BDT classifier are chosen based on estimations of requirements that provide the best sensitivity to *CP*-violating observables. Each BDT classifier retains roughly $85 - 90\%$ of signal candidates and removes over 90% of combinatorial background.

Strict particle identification (PID) requirements are placed on the kaon child of the K^{*0} candidate as the charge of this particle is used to determine the flavour of the parent B meson. Less stringent particle identification requirements are also placed on the pion from the K^{*0} candidate and all kaons and pions from the two-body D meson decay candidates. For $D \to K\pi\pi\pi$ and $D \to \pi K\pi\pi$ decay candidates, the kaon and both pions with charge opposite to the D candidate kaon child are subject to PID requirements. For $D \to \pi\pi\pi\pi$ candidates, only the two pions with the same charge as the K^{*0} candidate kaon child are subject to PID requirements. All particles with PID requirements are also required to have track momentum between $3 - 200\,\mathrm{GeV}/c$ to ensure suitable discrimination between kaons and pions in the RICH detectors.

Requirements are also placed on the displacement of the D candidate decay vertex from the B^0 candidate decay vertex to suppress charmless B^0 decays to the same final states, which proceed without an intermediate D meson. Different requirements are placed on the ADS and GLW final states due to different relative contributions of these backgrounds. For the GLW (ADS) final states, the D candidate decay vertex displacement is required to be three (two) times its uncertainty. A discussion of the remaining contributions from

these charmless backgrounds is included in Sect. 4.1.

Finally, vetoes are applied to each D final state to remove backgrounds or maintain consistency with the measurements of D hadronic parameters used in Sect. 5. In the ADS final states, doubly-misidentified backgrounds are removed with the requirement that the D reconstructed mass where the mass hypotheses of the kaon and pion children have been swapped differs from the known D^0 meson mass by more than $15\,\mathrm{MeV}/c^2$. Backgrounds from $B^\pm \to DK^\pm$ decays paired with a random pion are removed with a requirement that the $DK^\pm$ reconstructed mass be more than $25\,\mathrm{MeV}/c^2$ away from the known $B^\pm$ meson mass. Decays of the B^0 meson to the same final state proceeding through different charmed intermediate states, *e.g.* $B^0 \to D^-[K^+\pi^-\pi^-]\pi^+$ misidentified as $B^0 \to D[\pi^+\pi^-]K^+\pi^-$, are removed with requirements that the reconstructed mass of a D-child combined with the K^{*0} candidate to form a Cabibbo-favoured decay of another charmed meson does not fall within $15\,\mathrm{MeV}/c^2$ of the known meson mass. Candidate $D \to K^0_S\pi^+\pi^-$ decays are removed from the $D \to \pi^+\pi^-\pi^+\pi^-$ sample with the requirement that the reconstructed $\pi^+\pi^-$ masses are not within $480 - 505\,\mathrm{MeV}/c^2$.

The *CP*-violating observables of interest are all proportional to the ratios of decay rates of different D final states, and thus much of the reconstruction and selection efficiency cancels in these ratios. However, due to the different kinematic distributions of each D final state, and due to different selection requirements placed on the different D decay modes, these efficiencies must be accounted for. Additionally, effects introducing asymmetries aside from those due to the interference discussed in Sect. 1 must be corrected for.

The selection requirements are applied to simulated samples to estimate the selection efficiencies of each final state integrated across the two B flavours, with the exception of PID efficiencies. Charge-dependent PID efficiencies are estimated with calibration data samples of kaons and pions collected from D^* decays weighted to match the kinematics of signal decays predicted by simulation.

Three other possible sources of flavour asymmetry must be accounted for, aside from that resulting from the interference discussed in Sect. 1. First, an asymmetry can be introduced in the production of B^0 mesons and $\overline{B}^0$ mesons from the initial proton-proton collisions, referred to as A_{prod}. Second, tracking and reconstruction can depend on the charge of final state particles due to the difference of interactions between particles and anti-particles and the detector material, which is accounted for through the difference in detection asymmetry between kaons and pions $A_{K\pi} = A_K - A_\pi$. Lastly, similar to above, asymmetries can be introduced in PID which is accounted for implicitly in the PID efficiency corrections discussed previously.

The parameter A_{prod} is determined from the measurement of B^0 and B^0_s asymmetries in Ref. [33]. The measured production asymmetries are $A_{\mathrm{prod}} = (-8 \pm 5) \times 10^{-3}$ and $A_{s,\mathrm{prod}} = (6 \pm 10) \times 10^{-3}$. Since these results are only determined using data from pp centre-of-mass energies of 7 and 8 TeV, and not at 13 TeV, the same central value is assumed for the full dataset.

The value of $A_{K\pi}$ is estimated using calibration data samples of $D^+ \to K^-\pi^+\pi^+$ and $D^+ \to K^0_S\pi^+$ decays. The resulting predicted asymmetry weighted to match the signal kinematic distributions is $A_{K\pi} = (-9.8 \pm 5.5) \times 10^{-3}$. The total detection asymmetry for a $B^0 \to DK^{*0}$ candidate depends on the difference between the number of kaons and the number of pions of the same sign in the final state, *e.g.* the $B^0 \to D[K\pi]K^{*0}$ final state is corrected by $2A_{K\pi}$, the $B^0 \to D[\pi\pi]K^{*0}$ final state is corrected by $A_{K\pi}$, and the $B^0 \to D[\pi K]K^{*0}$ final state requires no such correction. The effects of imperfect modeling

in simulation of the kinematic distributions of the four-body D decays were investigated and found to be negligible.

4 Measurement of *CP*-violating observables

The *CP*-violating observables discussed in Sect. 1 are determined from the selected data through a simultaneous unbinned extended maximum-likelihood fit of the B^0 candidate reconstructed mass for each flavour of each D final state, where constraints are placed on the D candidate mass and the direction of the B candidate momentum using the DecayTreeFitter package [34]. This reconstructed mass is calculated with these constraints unless otherwise specified.

4.1 Modelling the reconstructed mass distribution

The reconstructed mass distributions of both $B^0 \to DK^{*0}$ and $B^0_s \to D\overline{K}^{*0}$ decays are modelled by modified Cruijff functions [35] parameterised as

$$f(M) = \begin{cases} e^{\frac{-(M-\mu)^2\left(1+\beta(M-\mu)^2\right)}{2\sigma^2+\alpha_L(M-\mu)^2}}, & M < \mu \\ e^{\frac{-(M-\mu)^2\left(1+\beta(M-\mu)^2\right)}{2(\rho\sigma)^2+\alpha_R(M-\mu)^2}}, & M > \mu \end{cases}. \tag{6}$$

All the parameters of the $B^0_{(s)} \to DK^{*0}$ modified Cruijff functions are fixed from fits to the corresponding simulation samples of $B^0_{(s)} \to D([K\pi])([\pi K])K^{*0}$, with the exception of the μ and σ parameters, which are left as free parameters in the probability distribution functions (PDFs) describing the B^0 and B^0_s mesons. The constraints on the D meson mass minimise the dependence on the D decay final state, but an additional correction factor determined from simulation is applied to the width for the PDFs describing the reconstructed mass distributions of the four-body D final states.

The selection requirements accept $B^0_{(s)} \to D^*K^{*0}$ decays with a similar efficiency to signal decays, as their topology is identical to signal decays with one additional missing neutral particle from the $D^* \to \gamma/\pi^0 D$ decay. The reconstructed mass of these decays are mainly located below the B^0 mass peak, but the right-hand tail of the $B^0_s \to D^*\overline{K}^{*0}$ distribution extends to the B^0 meson mass. As this is the decay of a pseudoscalar particle into two vector particles, the final state is characterised by three independent helicity (0, ±1) amplitudes. However, two of these amplitudes (±1) have indistinguishable reconstructed mass distributions. This leaves four different configurations of $B^0 \to D^*K^{*0}$ decays: two possible D^* decay chains each with two reconstructed mass distributions. Each configuration is modelled with either a single broad peaking structure or a double-peaked structure, as described in Ref. [36]. The relative size of the $D^*[\gamma D]$ and $D^*[\pi^0 D]$ decays in helicity state 0 are fixed based on efficiencies predicted from simulation and the measured branching fractions. The same is done for the decays in helicity state ±1. The interference effects of interest can affect the helicity amplitudes differently. Therefore, four free parameters are included in the fit to account for this: one for the ratio of helicity states in ADS $B^0 \to D^*K^{*0}$ decays, one ratio for each flavour of the GLW $B^0 \to D^*K^{*0}$ decays, and one ratio shared across all $B^0_s \to D^*\overline{K}^{*0}$ final states.

Due to particle misidentification, $B^0 \to D\pi^+\pi^-$ decays can also be mistaken for signal decays when one pion is misidentified as a kaon, as can $B^0 \to D^*\pi^+\pi^-$ decays. The relatively stringent PID requirement on the K^+ child of the K^{*0} suppresses these contributions significantly, but not to negligible levels. The reconstructed mass distribution of these decays is taken from simulated samples with PID weights determined from calibration data samples. The simulation samples only consider the contribution of $B^0 \to D\rho^0[\pi^+\pi^-]$ and $B^0 \to D^*\rho^0[\pi^+\pi^-]$, as the selection requirements on the K^{*0} candidate significantly suppress other contributions. The reconstructed mass distribution of $B^0 \to D\rho^0[\pi^+\pi^-]$ decays is modelled with a double-sided Crystal Ball PDF [37]. The PDF for $B^0 \to D^*\rho^0[\pi^+\pi^-]$ decays is parameterised in a similar fashion to the $B^0 \to D^{*0}K^{*0}$ decays, and the PDF shares the ratio of helicity states with ADS $B^0 \to D^*K^{*0}$ decays. The peak of the $B^0 \to D\rho^0[\pi^+\pi^-]$ distribution is located between the B^0 and B_s^0 peaks, while the $B^0 \to D^*\rho^0[\pi^+\pi^-]$ distribution has minimal contribution near or above the B^0 mass peak.

Partially reconstructed $B^+ \to DK^+\pi^+\pi^-$ decays, where the π^+ is not included in the reconstruction, also pass final selection requirements. A variety of intermediate decay chains can contribute to the final state. Based on the results of [38], the assumption is made that $B^+ \to DK^+\pi^+\pi^-$ decays are dominated by the process $B^+ \to DK_1(1270)^+$, due to the observably significant presence of both the ρ^0 and $K^*(892)^0$ resonances. The reconstructed mass distribution of these decays is modelled with a smoothed kernel density estimation [39] of simulated $B^+ \to DK_1(1270)^+$ decays, and contributes negligibly near the B^0 mass peak, being distributed primarily around a reconstructed mass of 5050 MeV/c^2.

Requirements placed on the D candidate flight significance do not fully suppress the contribution of charmless B^0 and B_s^0 decays to the same final state. The size of these contributions and possible flavour asymmetries in each final state are estimated based on the data, using candidates in the sideband of the D candidate reconstructed mass. Fits are performed to the B^0 candidate reconstructed mass without any constraints on the D candidate to determine the yields in the sideband regions for each final state and infer the expected number of these decays that pass selection requirements. The magnitude of flavour asymmetry in these decays is estimated with a similar procedure, however with a significantly less stringent requirement on the D flight significance to increase statistical precision. Significant charmless contributions from B_s^0 decays are only observed in the $D \to \pi K$ and $D \to \pi K\pi\pi$ final states. The results of these estimations are shown in Table 1.

Table 1: Estimated charmless contributions by D decay and B flavour.

D Mode	$\overline{B}^0$ Yields	B^0 Yields	B_s^0 Yields	$\overline{B}_s^0$ Yields
$K\pi$	-0.3 ± 0.2	-0.3 ± 0.2	0	0
πK	11.8 ± 2.4	16.6 ± 3.4	18.7 ± 2.9	19.8 ± 3.1
$\pi\pi$	12.8 ± 3.6	11.0 ± 3.0	0	0
KK	7.6 ± 2.6	7.6 ± 2.6	0	0
$K\pi\pi\pi$	2.3 ± 2.3	2.3 ± 2.3	0	0
$\pi K\pi\pi$	11.5 ± 1.9	5.2 ± 4.3	13.3 ± 3.1	14.2 ± 3.3
$\pi\pi\pi\pi$	9.8 ± 4.0	8.6 ± 3.5	0	0

The combinatorial background is modelled by an exponential PDF. The parameters of

the exponential PDF associated with each D decay mode vary freely in the fit, but are shared across B flavour for each D decay mode.

4.2 Reconstructed mass fit parameterisation

The fit to determine the number of signal decays in each of the fourteen samples (two flavours for each of the seven D final states) is parameterised in terms of the *CP*-violating observables introduced in Sect. 1, the flavour-integrated number of observed $B^0 \to D[K\pi]K^{*0}$ decays, and the flavour-integrated number of observed $B^0 \to D[K\pi\pi\pi]K^{*0}$ decays. These observables are related to the number of observed decays in each signal mode and the efficiency and asymmetry corrections discussed in Sect. 4.1. The $\mathcal{R}_{CP}^{hh(\pi\pi)}$ parameters are dependent on measured D^0 branching fractions. The values of the input branching fractions and the measured uncertainties are shown in Table 2.

Table 2: Summary of all branching fractions used as inputs in the measurement with uncertainties.

Branching Fraction	Value	
$\mathcal{B}(D^0 \to K^-\pi^+)$	$(3.999 \pm 0.045)\,\%$	[6]
$\mathcal{B}(D^0 \to \pi^+\pi^-)$	$(1.490 \pm 0.027) \times 10^{-3}$	[6]
$\mathcal{B}(D^0 \to K^+K^-)$	$(4.113 \pm 0.051) \times 10^{-3}$	[6]
$\mathcal{B}(D^0 \to K^-\pi^+\pi^+\pi^-)$	$(8.22 \pm 0.14)\,\%$	[31]
$\mathcal{B}(D^0 \to \pi^+\pi^-\pi^+\pi^-)$	$(7.56 \pm 0.20) \times 10^{-3}$	[31]

The $B_s^0 \to D\overline{K}^{*0}$, $B^0 \to D^*K^{*0}$, $B_s^0 \to D^*\overline{K}^{*0}$, and $B^+ \to DK^+\pi^+\pi^-$ background components are parameterised in a similar fashion. The *CP*-violating observables of $B_s^0 \to D\overline{K}^{*0}$ are left as free parameters in the fit, as are the *CP*-violating observables of $B^0 \to D^*K^{*0}$ decays. The observables of $B_s^0 \to D^*\overline{K}^{*0}$ are fixed to have no effects from interference, and the *CP*-violating observables of $B^+ \to DK^+\pi^+\pi^-$ decays are fixed to the measurements for the two-body D final states from [38] and predicted values based on the results of [7] for the four-body D final states. The $B^0 \to D\pi^+\pi^-$ and $B^0 \to D^*\pi^+\pi^-$ yields are constrained across different decay modes based on the yields of these backgrounds that are observed in $B^0 \to D[K\pi]K^{*0}$, but scaled with the relative D branching fractions and efficiencies, except for $B^0 \to D[\pi K]K^{*0}$ decays, where the yield is constrained to the same value as that in $B^0 \to D[K\pi]K^{*0}$, due to an equal probability of misidentifying the π^+ and the π^-. The number of charmless decays are subject to Gaussian constraints according to the values determined in Table 1. The combinatorial backgrounds are paramaterised simply in terms of the observed number of candidates, which is required to be equal for each flavour of a given D decay mode. The possibility of biases introduced in the fitting procedure is investigated by fitting toy data samples generated from the result of the total PDF fit to data. No evidence is seen for biases in the central values or uncertainties of any of the *CP*-violating observables.

4.3 Systematic uncertainties

The following sources of systematic uncertainties are considered: uncertainty in the determination of the asymmetry and efficiency corrections, uncertainty from the measured

branching fractions used as inputs in the fit, and uncertainty in the modelling of the PDFs or in the determination of the fixed yields in the fit. Any systematic uncertainties that are estimated at less than 5% of the measured statistical uncertainty from the fit are considered negligible, and are ignored in the final determination of systematic uncertainties. A summary of the assigned systematic uncertainties is provided in Table 3. All discussed sources are added in quadrature. The dominant systematic uncertainties are due to the measurement of input branching fractions and asymmetry corrections, but are generally small compared to statistical uncertainties.

The uncertainties of $A_{\rm prod}$ and $A_{K\pi}$ are propagated to the parameters of interest based on the quoted uncertainties in Sect. 3. The measured uncertainty of $A_{\rm prod}$ [33] is doubled for the data samples collected at 13 TeV to account for possible energy-dependence in the asymmetry. Additionally, the possibility of asymmetries introduced by the LHCb hardware trigger are accounted for, estimated to be at the level of 10^{-3} based on the results of [36]. The uncertainty due to the selection efficiencies largely cancels, with the primary non-cancelling uncertainty arising from different PID requirements on different final states. Uncertainties are determined due to the estimated PID efficiencies due to the limited statistics of simulated samples for kinematic weighting, and the finite size of bins used in the weighting of the PID efficiency. The propagated uncertainties of the input branching fractions listed in Table 2 are also determined.

The uncertainty due to the modelling of the B^0 candidate reconstructed mass for each component in the fit is also investigated. The uncertainty due to the modelling of $B^0_s \to D^* K^{*0}$ decays is assessed by varying the determined efficiencies and input branching fractions of the $D^*[\gamma D]$ and $D^*[\pi^0 D]$ components within their respective uncertainties. Two alternative PDFs are examined to assess uncertainty in the modelling of $B^+ \to DK^+\pi^+\pi^-$ decays: one based on simulated samples of $B^+ \to DK^*(1400)^0[K^+\pi^+\pi^-]$ decays, and another based on $B^+ \to DK^+\pi^+\pi^-$ decays collected from data. Performing the fit with either distribution results in negligible variations in the *CP*-violating observables. An alternate $B^0 \to D\pi^+\pi^-$ reconstructed mass distribution composed of an equal admixture of $B^0 \to D\rho^0[\pi^+\pi^-]$ and non-resonant $B^0 \to D\,(\pi\pi)_{S-\rm wave}$ decays based on results in Ref. [40] is also considered. These uncertainties are negligible for all *CP*-violating observables except $R^{\pm}_{\pi K(\pi\pi)}$.

The statistical uncertainty of the flavour-integrated number of charmless decays is accounted for through Gaussian constraints in the fit, but the asymmetry of the charmless yields is fixed based on the central values determined in data. The resulting uncertainty on the parameters of interest is determined through variations of the charmless asymmetries within their measured uncertainties.

	$\mathcal{A}_{K\pi}$	$\mathcal{R}^{+}_{\pi K}$	$\mathcal{R}^{-}_{\pi K}$	$\mathcal{R}^{\pi\pi}_{CP}$	$\mathcal{A}^{\pi\pi}_{CP}$	$\mathcal{R}^{KK}_{CP}$	$\mathcal{A}^{KK}_{CP}$	$\mathcal{A}_{K\pi\pi\pi}$	$R^{+}_{\pi K\pi\pi}$	$\mathcal{R}^{-}_{\pi K\pi\pi}$	$\mathcal{R}^{4\pi}_{CP}$	$\mathcal{A}^{4\pi}_{CP}$
$A_{\rm prod}$	0.009	0.001	0.001	0.002	0.009	–	0.009	0.009	0.001	0.001	–	0.009
$A_{K\pi}$	0.009	0.001	0.001	0.001	0.006	0.001	0.006	0.009	0.001	0.001	0.001	0.006
PID	0.008	0.004	0.004	0.012	0.010	0.010	0.010	0.010	0.004	0.004	0.017	0.011
Fit PDFs	–	0.003	0.003	–	–	–	–	–	0.003	0.003	–	–
Charmless Asymmetries	–	–	–	0.011	0.005	–	–	–	0.001	0.001	–	–
Input Branching Fractions	–	–	–	0.020	–	0.013	–	–	–	–	0.028	–
$\sigma_{\rm sys}$	0.015	0.005	0.005	0.026	0.016	0.017	0.015	0.016	0.005	0.005	0.033	0.016
$\sigma_{\rm stat}$	0.017	0.013	0.013	0.110	0.103	0.057	0.064	0.018	0.014	0.014	0.084	0.088

Table 3: Summary of uncertainties on the physics observables measured in $B^0 \to DK^{*0}$ decays. Uncertainties less than $0.05\sigma_{\rm stat.}$ are indicated with dashed lines.

4.4 Results of the reconstructed mass fit

The results of the fit are shown in Figs. 1–3. The yields of the favoured decays, $N_{K\pi}$, $N_{K\pi\pi\pi}$, $N_{s,\pi K}$, and $N_{s,\pi K\pi\pi}$ are found to be roughly 3800, 3600, 8800, and 8200, respectively. The *CP*-violating observables determined in the fit for $B^0 \to DK^{*0}$ decays are given in Table 4 and the results of $B^0_s \to D\overline{K}^{*0}$ are given in Table 5. The results from the B^0_s decays conform to the expectation of unobservable effects of interference – all $\mathcal{R}^s_{CP}$ parameters are consistent with unity within one standard deviation, and no statistically significant asymmetries are observed. However, statistically significant evidence of interference is seen in the $B^0 \to DK^{*0}$ results, most notably in $\mathcal{R}^{KK}_{CP}$ at 3σ. An approximately 2σ tension is observed between the values of $\mathcal{R}^{KK}_{CP}$ and $\mathcal{R}^{\pi\pi}_{CP}$, which are expected to be consistent, but this difference is attributed to a statistical fluctuation. The asymmetries $\mathcal{A}^{KK}_{CP}$ and $\mathcal{A}^{\pi\pi}_{CP}$ are consistent with each other. In aggregate, the results are self-consistent, as evidenced by our interpretation of the parameters in Sect. 5.

Statistical uncertainties on the *CP*-violating observables have been reduced by around 60% in comparison to the previous results in Ref. [13], which is consistent with the increase in signal yield. Central values are also consistent taking into account correlations and the ability with the larger dataset to determine the contribution of charmless decays more accurately.

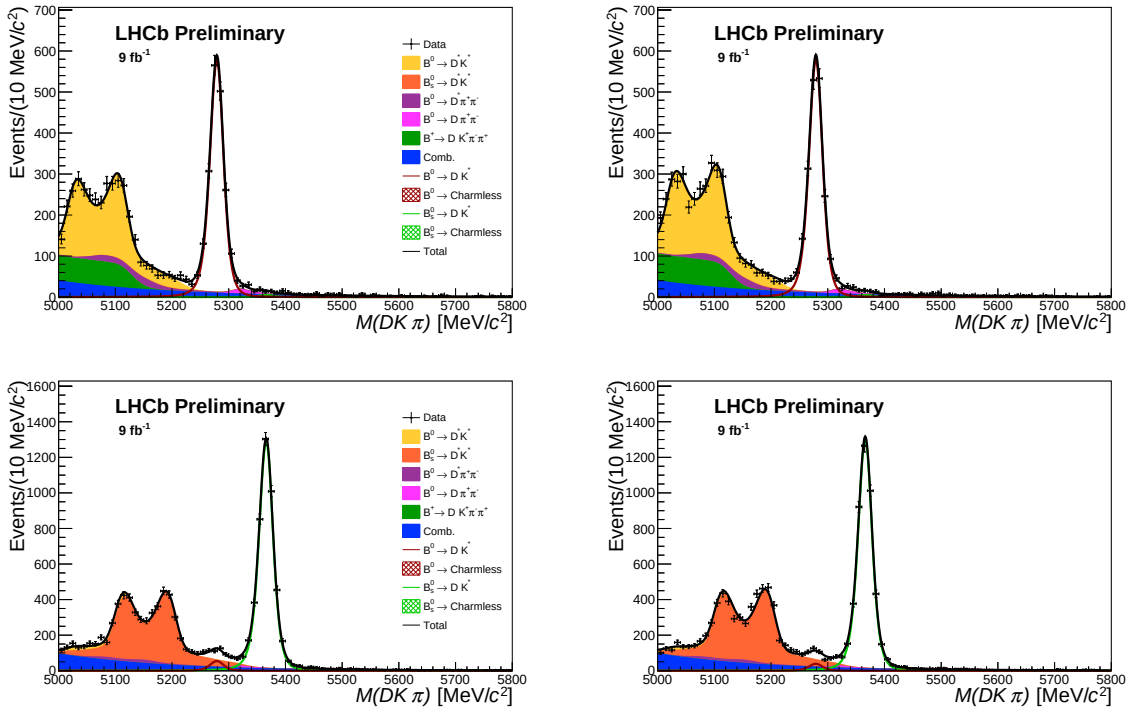

Figure 1: Reconstructed mass distributions for selected candidates in the (left) $\overline{B}^0$ and (right) B^0 samples for the (top) $D \to K\pi$ and (bottom) $D \to \pi K$ decay channels. The fit projection is overlaid.

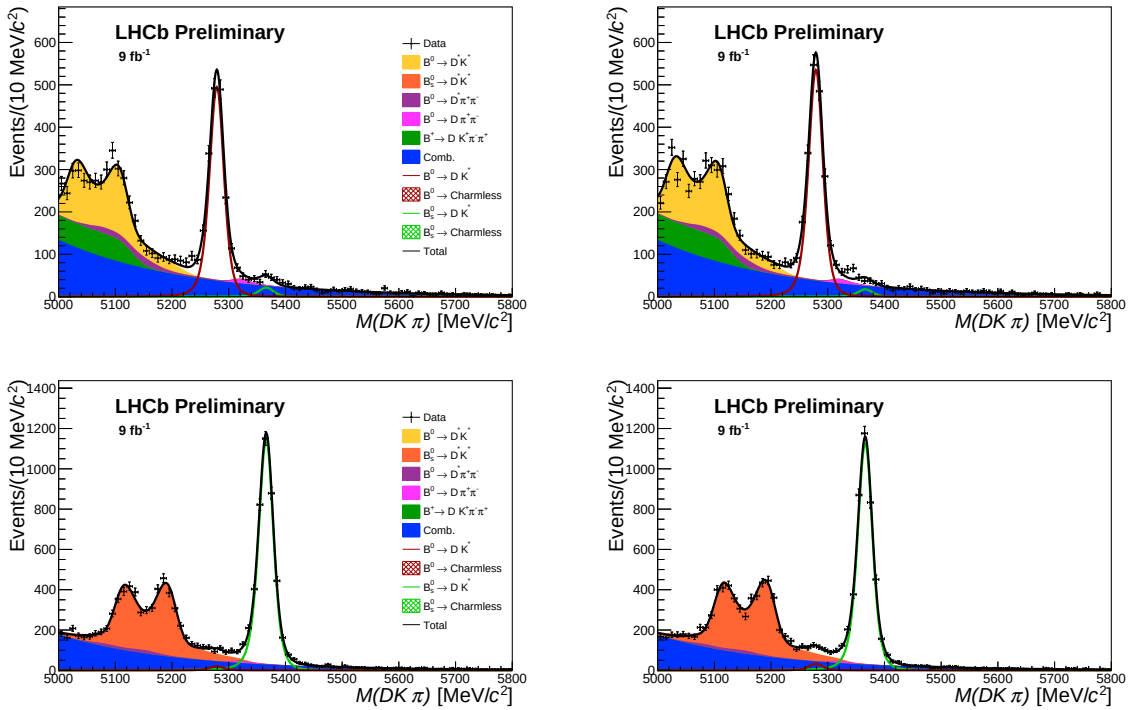

Figure 2: Reconstructed mass distributions for selected candidates in the (left) $\overline{B}^0$ and (right) B^0 samples for the (top) $D \to K\pi\pi\pi$ and (bottom) $D \to \pi K\pi\pi$ decay modes. The fit projection is overlaid.

Table 4: Fitted physics parameters relating to $B^0 \to DK^{*0}$ decays. The first stated uncertainties are statistical and the second are systematic.

Parameter	Value
$\mathcal{A}_{K\pi}$	$0.033 \pm 0.017 \pm 0.015$
$\mathcal{R}^+_{\pi K}$	$0.069 \pm 0.013 \pm 0.005$
$\mathcal{R}^-_{\pi K}$	$0.093 \pm 0.013 \pm 0.005$
$\mathcal{A}_{K\pi\pi\pi}$	$-0.010 \pm 0.018 \pm 0.016$
$\mathcal{R}^+_{\pi K\pi\pi}$	$0.060 \pm 0.014 \pm 0.005$
$\mathcal{R}^-_{\pi K\pi\pi}$	$0.038 \pm 0.014 \pm 0.005$
$\mathcal{R}^{KK}_{CP}$	$0.817 \pm 0.057 \pm 0.017$
$\mathcal{A}^{KK}_{CP}$	$-0.047 \pm 0.063 \pm 0.015$
$\mathcal{R}^{\pi\pi}_{CP}$	$1.085 \pm 0.110 \pm 0.026$
$\mathcal{A}^{\pi\pi}_{CP}$	$-0.034 \pm 0.094 \pm 0.016$
$\mathcal{R}^{4\pi}_{CP}$	$0.882 \pm 0.086 \pm 0.033$
$\mathcal{A}^{4\pi}_{CP}$	$0.014 \pm 0.087 \pm 0.016$

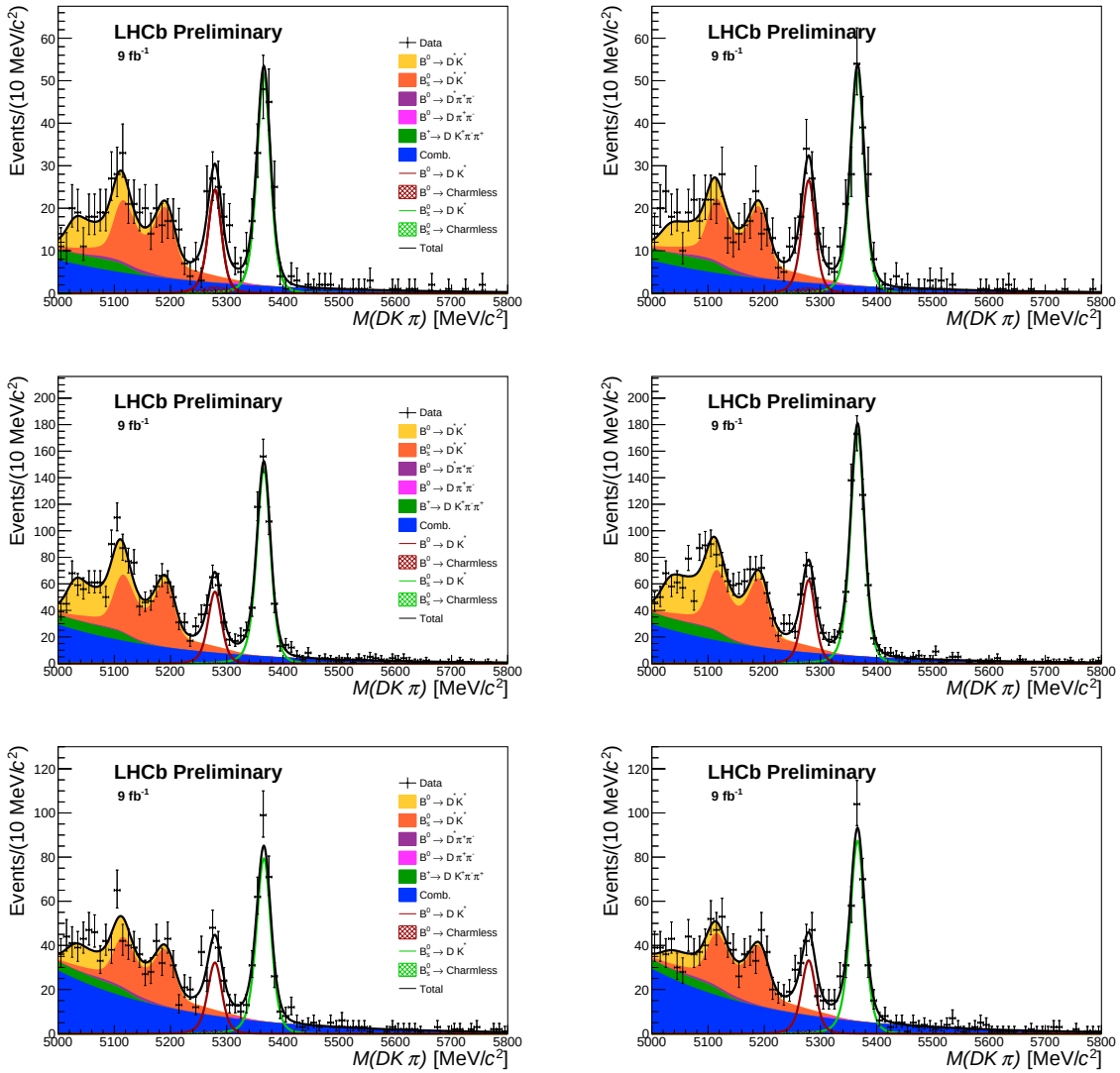

Figure 3: Reconstructed mass distributions for selected candidates in the (left) $\overline{B}^0$ and (right) B^0 samples for the (top) $D \to \pi\pi$, (centre) $D \to KK$, and (bottom) $D \to \pi\pi\pi\pi$ decay modes. The fit projection is overlaid.

5 Interpretation and conclusions

The measured parameters determined from Table 4 can be expressed in terms of the fundamental physics parameters of interest, γ, $r_{B^0}^{DK^*}$, and $\delta_{B^0}^{DK^*}$, and some additional inputs. These additional inputs include the coherence factor κ_{B^0}, which quantifies the dilution of the interference effects of interest due to the selected $B^0 \to DK^+\pi^-$ decays that do not proceed through an intermediate K^{*0} resonance. The value of this parameter measured by [30] is used, which placed identical requirements on the K^{*0} candidate to those presented in this article. There is additional dependence on the hadronic parameters associated with the D meson decays to a final state X: r_D^X, δ_D^X, and κ_D^X for ADS decays, and the CP-even fraction F_+^X for GLW decays. The values of the ADS parameters are taken from [7] for the $D \to K\pi$ decay and from [41] for the $D \to K\pi\pi\pi$ decay. For the two-body GLW modes, $F_+^{hh} = 1$, and the value of $F_+^{4\pi} = 0.737 \pm 0.028$ is taken from [42].

Table 5: Fitted physics parameters relating to $B_s^0 \to D\overline{K}^{*0}$ decays. The first stated uncertainties are statistical and the second are systematic.

Parameter	Value
$\mathcal{A}_{s,\pi K}$	$-0.012 \pm 0.011 \pm 0.020$
$\mathcal{R}^{+}_{s,K\pi}$	$0.004 \pm 0.002 \pm 0.006$
$\mathcal{R}^{-}_{s,K\pi}$	$0.004 \pm 0.002 \pm 0.006$
$\mathcal{A}_{s,\pi K\pi\pi}$	$-0.031 \pm 0.012 \pm 0.021$
$\mathcal{R}^{+}_{s,K\pi\pi\pi}$	$0.019 \pm 0.004 \pm 0.006$
$\mathcal{R}^{-}_{s,K\pi\pi\pi}$	$0.015 \pm 0.004 \pm 0.006$
$\mathcal{R}^{s,KK}_{CP}$	$1.004 \pm 0.034 \pm 0.016$
$\mathcal{A}^{s,KK}_{CP}$	$0.063 \pm 0.032 \pm 0.021$
$\mathcal{R}^{s,\pi\pi}_{CP}$	$0.982 \pm 0.057 \pm 0.023$
$\mathcal{A}^{s,\pi\pi}_{CP}$	$-0.003 \pm 0.056 \pm 0.021$
$\mathcal{R}^{s,4\pi}_{CP}$	$1.017 \pm 0.048 \pm 0.033$
$\mathcal{A}^{s,4\pi}_{CP}$	$0.022 \pm 0.044 \pm 0.022$

The GLW observables $\mathcal{A}_{CP}^{hh(\pi\pi)}$ and $\mathcal{R}_{CP}^{hh(\pi\pi)}$ relate to these parameters through

$$\begin{aligned}
\mathcal{A}_{CP}^{hh(\pi\pi)} &= \frac{2\kappa_{B^0} r_{B^0}^{DK^*}\left(2F_+^{hh(\pi\pi)}-1\right)\sin\left(\delta_{B^0}^{DK^*}\right)\sin(\gamma)}{1+(r_{B^0}^{DK^*})^2+2\kappa_{B^0}\cos\left(\delta_{B^0}^{DK^*}\right)\cos(\gamma)} \text{ and} \\
\mathcal{R}_{CP}^{hh(\pi\pi)} &= \frac{1+(r_{B^0}^{DK^*})^2+2\kappa_{B^0} r_{B^0}^{DK^*}\left(2F_+^{hh(\pi\pi)}-1\right)\cos\left(\delta_{B^0}^{DK^*}\right)\cos(\gamma)}{1+(r_{B^0}^{DK^*})^2\left(r_D^{K\pi\pi\pi}\right)^2+2\kappa_{B^0} r_{B^0}^{DK^*} r_D^{K\pi\pi\pi}\kappa_D^{K\pi\pi\pi}\cos\left(\delta_{B^0}^{DK^*}-\delta_D^{K\pi\pi\pi}\right)\cos(\gamma)}.
\end{aligned} \tag{7}$$

The $\mathcal{R}^{+}_{\pi K(\pi\pi)}$ and $\mathcal{R}^{-}_{\pi K(\pi\pi)}$ observables can be expressed, neglecting effects of charm mixing, as

$$\mathcal{R}^{\pm}_{\pi K(\pi\pi)} = \frac{(r_{B^0}^{DK^*})^2 + \left(r_D^{K\pi(\pi\pi)}\right)^2 + 2\kappa_{B^0} r_{B^0}^{DK^*} r_D^{K\pi(\pi\pi)}\kappa_D^{K\pi(\pi\pi)}\cos\left(\delta_{B^0}^{DK^*} + \delta_D^{K\pi(\pi\pi)} \pm \gamma\right)}{1 + (r_{B^0}^{DK^*})^2\left(r_D^{K\pi(\pi\pi)}\right)^2 + 2\kappa_{B^0} r_{B^0}^{DK^*} r_D^{K\pi(\pi\pi)}\kappa_D^{K\pi(\pi\pi)}\cos\left(\delta_{B^0}^{DK^*} - \delta_D^{K\pi(\pi\pi)} \pm \gamma\right)}, \tag{8}$$

where $\kappa_D^{K\pi} = 1$. Additional corrections are made due to the effects of charm mixing, as described in Ref. [43], which are on the order of 1%. Finally, the parameters $\mathcal{A}_{K\pi}$ and $\mathcal{A}_{K\pi\pi\pi}$ can be expressed as

$$\mathcal{A}_{K\pi(\pi\pi)} = \frac{2\kappa_{B^0}\kappa_D^{K\pi(\pi\pi)} r_D^{K\pi(\pi\pi)}\sin\left(\delta_{B^0}^{DK^*} - \delta_D^{K\pi(\pi\pi)}\right)\sin(\gamma)}{1 + (r_{B^0}^{DK^*})^2\left(r_D^{K\pi(\pi\pi)}\right)^2 + 2\kappa_{B^0}\kappa_D^{K\pi(\pi\pi)} r_D^{K\pi(\pi\pi)}\cos\left(\delta_{B^0}^{DK^*} - \delta_D^{K\pi(\pi\pi)}\right)\cos(\gamma)}. \tag{9}$$

With Eqns. 7–9, the measured *CP*-violating observables from Table 4, and the aforementioned inputs, limits are set on the (γ, $r_{B^0}^{DK^*}$, $\delta_{B^0}^{DK^*}$) parameter space using the GammaCombo package [44]. The correlations of statistical and systematic uncertainties for the measured *CP*-violating observables are accounted for with correlation matrices shown in App. A. Four solutions are found, and constraints on the parameter space are shown in Figs. 4–7. The preferred solution determines γ to be roughly 172° with an uncertainty around 6° and $\delta_{B^0}^{DK^*}$ to be roughly 296° with an uncertainty around 8°. However, the

second-preferred solution is consistent with the world-average of direct measurements of $\gamma = \left(66.2^{+3.4}_{-3.6}\right)^\circ$ [6], finding γ to be roughly 62° with around 8° of uncertainty and $\delta_{B^0}^{DK^*}$ to be roughly 187° with around 6° of uncertainty. The results of $B^0 \to D[K^0_S h^+ h^-]K^{*0}$ [45] break the degeneracy of these two solutions, indicating a strong preference for the solution consistent with the world-average. As can be seen in Figs. 5 and 6, all solutions give a consistent determination of $r_{B^0}^{DK^*}$, with the preferred solution of this analysis finding $r_{B^0}^{DK^*} = 0.235 \pm 0.018$.

In summary, measurements of *CP*-violating observables in $B^0 \to DK^{*0}$ decays are presented in this article. These are the most precise measurements to date and provide the most stringent limits to date on γ from B^0 decays. A solution for γ is found that is consistent with the measurement from B^+ decays reported in Ref. [6].

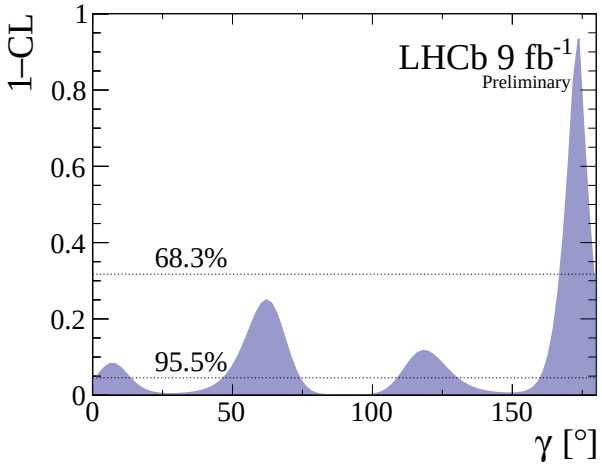

Figure 4: Confidence level contours from the fitted results of the B^0-related *CP*-violating observables projected to the γ axis.

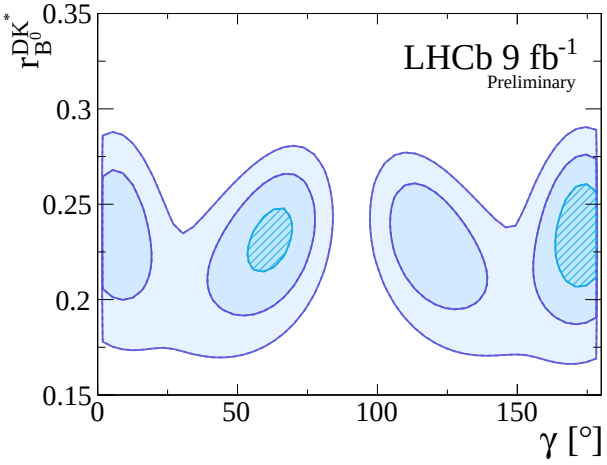

Figure 5: Confidence level contours from the fitted results of the B^0-related *CP*-violating observables projected to the γ-$r_{B^0}^{DK^{*0}}$ plane. Contours contain 68.3%, 95.4%, and 99.7% of the distribution.

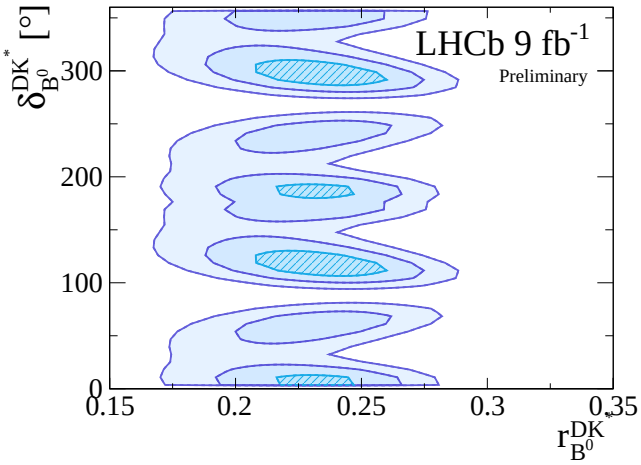

Figure 6: Confidence level contours from the fitted results of the B^0-related *CP*-violating observables projected to the $r_{B^0}^{DK^{*0}}$-$\delta_{B^0}^{DK^{*0}}$ plane. Contours contain 68.3%, 95.4%, and 99.7% of the distribution.

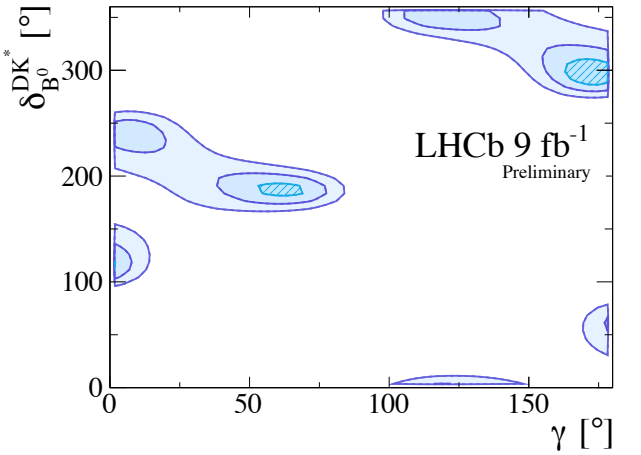

Figure 7: Confidence level contours from the fitted results of the B^0-related *CP*-violating observables projected to the γ-$\delta_{B^0}^{DK^{*0}}$ plane. Contours contain 68.3%, 95.4%, and 99.7% of the distribution.

References

[1] N. Cabibbo, *Unitary symmetry and leptonic decays*, Phys. Rev. Lett. **10** (1963) 531.

[2] M. Kobayashi and T. Maskawa, *CP-violation in the renormalizable theory of weak interaction*, Prog. Theor. Phys. **49** (1973) 652.

[3] J. Brod and J. Zupan, *The ultimate theoretical error on γ from $B \to DK$ decays*, JHEP **01** (2014) 051, arXiv:1308.5663.

[4] UTfit, M. Bona *et al.*, *New UTfit Analysis of the Unitarity Triangle in the Cabibbo-Kobayashi-Maskawa scheme*, Rend. Lincei Sci. Fis. Nat. **34** (2023) 37, arXiv:2212.03894.

[5] CKMfitter group, J. Charles *et al.*, *CP violation and the CKM matrix: Assessing the impact of the asymmetric B factories*, Eur. Phys. J. **C41** (2005) 1, arXiv:hep-ph/0406184, updated results and plots available at http://ckmfitter.in2p3.fr/.

[6] Heavy Flavor Averaging Group, HFLAV, Y. S. Amhis *et al.*, *Averages of b-hadron, c-hadron, and τ-lepton properties as of 2021*, Phys. Rev. D **107** (2023) 052008, arXiv:2206.07501.

[7] LHCb collaboration, *Simultaneous determination of the CKM angle γ and parameters related to mixing and CP violation in the charm sector*, LHCb-CONF-2022-003, 2022.

[8] T. Gershon, *On the measurement of the unitarity triangle angle γ from $B^0 \to DK^{*0}$ decays*, Phys. Rev. D **79** (2009) 051301.

[9] D. Atwood, I. Dunietz, and A. Soni, *Improved Methods for Observing CP Violation in $B^\pm \to KD$ and Measuring the CKM Phase γ*, Phys. Rev. D **63** (2001) 036005, arXiv:hep-ph/0008090.

[10] M. Gronau and D. Wyler, *On determining a weak phase from CP asymmetries in charged B decays*, Phys. Lett. B **265** (1991) 172.

[11] M. Gronau and D. London, *How to determine all the angles of the unitarity triangle from $B^0_d \to DK^0_S$ and $B^0_s \to D\phi$*, Phys. Lett. B **253** (1991) 483.

[12] M. Nayak *et al.*, *First determination of the CP content of $D \to \pi^+\pi^-\pi^0$ and $D \to K^+K^-\pi^0$*, Phys. Lett. B **740** (2015) 1, arXiv:1410.3964.

[13] LHCb collaboration, R. Aaij *et al.*, *Measurement of CP observables in the process $B^0 \to DK^{*0}$ with two- and four-body D decays*, JHEP **08** (2019) 041, arXiv:1906.08297.

[14] LHCb collaboration, R. Aaij *et al.*, *LHCb detector performance*, Int. J. Mod. Phys. **A30** (2015) 1530022, arXiv:1412.6352.

[15] LHCb collaboration, A. A. Alves Jr. *et al.*, *The LHCb detector at the LHC*, JINST **3** (2008) S08005.

[16] R. Aaij *et al.*, *Performance of the LHCb Vertex Locator*, JINST **9** (2014) P09007, arXiv:1405.7808.

[17] R. Arink *et al.*, *Performance of the LHCb Outer Tracker*, JINST **9** (2014) P01002, arXiv:1311.3893.

[18] M. Adinolfi *et al.*, *Performance of the LHCb RICH detector at the LHC*, Eur. Phys. J. **C73** (2013) 2431, arXiv:1211.6759.

[19] R. Aaij *et al.*, *Selection and processing of calibration samples to measure the particle identification performance of the LHCb experiment in Run 2*, Eur. Phys. J. Tech. Instr. **6** (2018) 1, arXiv:1803.00824.

[20] A. A. Alves Jr. *et al.*, *Performance of the LHCb muon system*, JINST **8** (2013) P02022, arXiv:1211.1346.

[21] V. V. Gligorov and M. Williams, *Efficient, reliable and fast high-level triggering using a bonsai boosted decision tree*, JINST **8** (2013) P02013, arXiv:1210.6861.

[22] T. Sjöstrand, S. Mrenna, and P. Skands, *PYTHIA 6.4 physics and manual*, JHEP **05** (2006) 026, arXiv:hep-ph/0603175.

[23] I. Belyaev *et al.*, *Handling of the generation of primary events in Gauss, the LHCb simulation framework*, J. Phys. Conf. Ser. **331** (2011) 032047.

[24] D. J. Lange, *The EvtGen particle decay simulation package*, Nucl. Instrum. Meth. **A462** (2001) 152.

[25] N. Davidson, T. Przedzinski, and Z. Was, *PHOTOS interface in C++: Technical and physics documentation*, Comp. Phys. Comm. **199** (2016) 86, arXiv:1011.0937.

[26] Geant4 collaboration, S. Agostinelli *et al.*, *Geant4: A simulation toolkit*, Nucl. Instrum. Meth. **A506** (2003) 250.

[27] Geant4 collaboration, J. Allison *et al.*, *Geant4 developments and applications*, IEEE Trans. Nucl. Sci. **53** (2006) 270.

[28] M. Clemencic *et al.*, *The LHCb simulation application, Gauss: Design, evolution and experience*, J. Phys. Conf. Ser. **331** (2011) 032023.

[29] G. A. Cowan, D. C. Craik, and M. D. Needham, *RapidSim: an application for the fast simulation of heavy-quark hadron decays*, Comput. Phys. Commun. **214** (2017) 239, arXiv:1612.07489.

[30] LHCb collaboration, R. Aaij *et al.*, *Constraints on the unitarity triangle angle γ from Dalitz plot analysis of $B^0 \to DK^+\pi^-$ decays*, Phys. Rev. **D93** (2016) 112018, Erratum ibid. **D94** (2016) 079902, arXiv:1602.03455.

[31] Particle Data Group, R. L. Workman and Others, *Review of particle physics*, Prog. Theor. Exp. Phys **2022** (2022) 083C01.

[32] J. Therhaag, *TMVA Toolkit for multivariate data analysis in ROOT*, PoS **ICHEP2010** (2010) 510.

[33] LHCb collaboration, R. Aaij *et al.*, *Measurement of B^0, B^0_s, B^+ and Λ^0_b production asymmetries in 7 and 8 TeV proton-proton collisions*, Phys. Lett. **B774** (2017) 139, arXiv:1703.08464.

[34] W. D. Hulsbergen, *Decay chain fitting with a Kalman filter*, Nucl. Instrum. Meth. **A552** (2005) 566, arXiv:physics/0503191.

[35] LHCb collaboration, R. Aaij *et al.*, *Measurement of the CKM angle γ in $B^\pm \to DK^\pm$ and $B^\pm \to D\pi^\pm$ decays with $D \to K^0_S h^+ h^-$*, JHEP **02** (2021) 0169, arXiv:2010.08483.

[36] LHCb collaboration, R. Aaij *et al.*, *Measurement of CP observables in $B^\pm \to D^{(*)}K^\pm$ and $B^\pm \to D^{(*)}\pi^\pm$ decays using two-body D final states*, JHEP **04** (2021) 081, arXiv:2012.09903.

[37] T. Skwarnicki, *A study of the radiative cascade transitions between the Upsilon-prime and Upsilon resonances*, PhD thesis, Institute of Nuclear Physics, Krakow, 1986, DESY-F31-86-02.

[38] LHCb collaboration, R. Aaij *et al.*, *Study of $B^- \to DK^-\pi^+\pi^-$ and $B^- \to D\pi^-\pi^+\pi^-$ decays and determination of the CKM angle γ*, Phys. Rev. **D92** (2015) 112005, arXiv:1505.07044.

[39] K. Cranmer, *Kernel Estimation in High-Energy Physics*, Computer Physics Communications (2001) 136:198, arXiv:hep-ex/0011057.

[40] LHCb collaboration, R. Aaij *et al.*, *Dalitz plot analysis of $B^0 \to \overline{D}^0\pi^+\pi^-$ decays*, Phys. Rev. **D92** (2015) 032002, arXiv:1505.01710.

[41] BESIII, M. Ablikim *et al.*, *Measurement of the $D \to K^-\pi^+\pi^+\pi^-$ and $D \to K^-\pi^+\pi^0$ coherence factors and average strong-phase differences in quantum-correlated $D\bar{D}$ decays*, JHEP **05** (2021) 164, arXiv:2103.05988.

[42] S. Malde *et al.*, *First determination of the CP content of $D \to \pi^+\pi^-\pi^+\pi^-$ and updated determination of the CP contents of $D \to \pi^+\pi^-\pi^0$ and $D \to K^+K^-\pi^0$*, Phys. Lett. B **747** (2015) 9, arXiv:1504.05878.

[43] M. Rama, *Effect of $D - \bar{D}$ mixing and CP violation in the measurement of γ with $B^\pm \to D^{(*)0}K^{(*)\pm}$ decays*, Nucl. Part. Phys. Proc. **273-275** (2016) 1436.

[44] LHCb collaboration, R. Aaij *et al.*, *Measurement of the CKM angle γ from a combination of LHCb results*, JHEP **12** (2016) 087, arXiv:1611.03076.

[45] LHCb collaboration, R. Aaij *et al.*, *TBD*, LHCb-PAPER-2023-009, in preparation.

A Correlation Matrices

The statistical correlation matrices of the determined CP-violating observables are shown in Table 6. The systematic correlations are shown in Table 7.

Table 6: Statistical correlation matrix of B^0 observables in percent. Values below the diagonal are implied by symmetry.

	$\mathcal{A}_{K\pi}$	$\mathcal{R}^+_{\pi K}$	$\mathcal{R}^-_{\pi K}$	$\mathcal{A}_{K\pi\pi\pi}$	$\mathcal{R}^+_{\pi K\pi\pi}$	$\mathcal{R}^-_{\pi K\pi\pi}$	$\mathcal{A}^{KK}_{CP}$	$\mathcal{R}^{KK}_{CP}$	$\mathcal{A}^{\pi\pi}_{CP}$	$\mathcal{R}^{\pi\pi}_{CP}$	$\mathcal{A}^{\pi\pi\pi\pi}_{CP}$	$\mathcal{R}^{\pi\pi\pi\pi}_{CP}$
$\mathcal{A}_{K\pi}$	100	9	−12	0	0	0	0	−1	0	0	0	0
$\mathcal{R}^+_{\pi K}$		100	6	0	0	0	0	3	0	2	0	0
$\mathcal{R}^-_{\pi K}$			100	0	0	0	0	3	0	2	0	0
$\mathcal{A}_{K\pi\pi\pi}$				100	7	−5	0	0	0	0	0	−1
$\mathcal{R}^+_{\pi K\pi\pi}$					100	8	0	0	0	0	0	2
$\mathcal{R}^-_{\pi K\pi\pi}$						100	0	0	0	0	0	1
$\mathcal{A}^{KK}_{CP}$							100	4	0	0	0	0
$\mathcal{R}^{KK}_{CP}$								100	0	5	0	0
$\mathcal{A}^{\pi\pi}_{CP}$									100	4	0	0
$\mathcal{R}^{\pi\pi}_{CP}$										100	0	0
$\mathcal{A}^{\pi\pi\pi\pi}_{CP}$											100	0
$\mathcal{R}^{\pi\pi\pi\pi}_{CP}$												100

Table 7: Sysematic correlation matrix of B^0 observables in percent. Values below the diagonal are implied by symmetry.

	$\mathcal{A}_{K\pi}$	$\mathcal{R}^+_{\pi K}$	$\mathcal{R}^-_{\pi K}$	$\mathcal{A}_{K\pi\pi\pi}$	$\mathcal{R}^+_{\pi K\pi\pi}$	$\mathcal{R}^-_{\pi K\pi\pi}$	$\mathcal{A}^{KK}_{CP}$	$\mathcal{R}^{KK}_{CP}$	$\mathcal{A}^{\pi\pi}_{CP}$	$\mathcal{R}^{\pi\pi}_{CP}$	$\mathcal{A}^{\pi\pi\pi\pi}_{CP}$	$\mathcal{R}^{\pi\pi\pi\pi}_{CP}$
$\mathcal{A}_{K\pi}$	100	0	−5	81	15	−19	78	−3	79	−3	78	−3
$\mathcal{R}^+_{\pi K}$		100	15	14	7	6	12	5	11	3	5	−1
$\mathcal{R}^-_{\pi K}$			100	−19	7	4	−26	14	−25	4	−26	−1
$\mathcal{A}_{K\pi\pi\pi}$				100	−1	−9	77	0	77	−1	76	−30
$\mathcal{R}^+_{\pi K\pi\pi}$					100	15	18	0	17	1	19	4
$\mathcal{R}^-_{\pi K\pi\pi}$						100	−24	0	−24	1	−23	4
$\mathcal{A}^{KK}_{CP}$							100	−3	94	−2	93	0
$\mathcal{R}^{KK}_{CP}$								100	−2	15	−1	−2
$\mathcal{A}^{\pi\pi}_{CP}$									100	−3	95	0
$\mathcal{R}^{\pi\pi}_{CP}$										100	−2	0
$\mathcal{A}^{\pi\pi\pi\pi}_{CP}$											100	−3
$\mathcal{R}^{\pi\pi\pi\pi}_{CP}$												100